Archives of Oral Biology 63 (2016) 93–105

Contents lists available at ScienceDirect

Archives of Oral Biology

journal homepage: www.elsevier.com/locate/aob

Distinct decalcification process of dentin by different cariogenic organic acids: Kinetics, ultrastructure and mechanical properties

Y-C Chien[a,b], A.K. Burwell[a], K. Saeki[a], A. Fernandez-Martinez[b,c], M.K. Pugach[a,1], G. Nonomura[a], S. Habelitz[a], S.P. Ho[a], M. Rapozo-Hilo[a], J.D. Featherstone[a], S.J. Marshall[a], G.W. Marshall[a,*]

[a] Division of Biomaterials and Bioengineering, Department of Preventive and Restorative Dental Sciences, University of California San Francisco, San Francisco, CA 94143-0758, US
[b] Molecular Foundry, Lawrence Berkeley National Laboratory, Berkeley, CA, US
[c] ISTerre, CNRS & University of Grenoble, B.P. 53X, Grenoble, Cedex 9, 38041, France

ARTICLE INFO

Article history:
Received 22 February 2015
Received in revised form 15 July 2015
Accepted 1 October 2015

Keywords:
Dentin caries models
Demineralization kinetics
AFM-nanoindenation
MicroXCT
TEM
SAXS

ABSTRACT

Objectives: We studied artificial dentin lesions in human teeth generated by lactate and acetate buffers (pH 5.0), the two most abundant acids in caries. The objective of this study was to determine differences in mechanical properties, mineral density profiles and ultrastructural variations of two different artificial lesions with the same approximate depth.
Methods: 0.05 M (pH 5.0) acetate or lactate buffer was used to create 1) 180 μm-deep lesions in non-carious human dentin blocks (acetate 130 h; lactate 14days); (2) demineralized, ~180 μm-thick non-carious dentin discs (3 weeks). We performed nanoindentation to determine mechanical properties across the hydrated lesions, and micro X-ray computed tomography (MicroXCT) to determine mineral profiles. Ultrastructure in lesions was analyzed by TEM/selected area electron diffraction (SAED). Demineralized dentin discs were analyzed by small angle X-ray scattering (SAXS).
Results: Diffusion-dominated demineralization was shown based on the linearity between lesion depths versus the square root of exposure time in either solution, with faster kinetics in acetate buffer. Nanoindentation revealed lactate induced a significantly sharper transition in reduced elastic modulus across the lesions. MicroXCT showed lactate demineralized lesions had swelling and more disorganized matrix structure, whereas acetate lesions had abrupt X-ray absorption near the margin. At the ultrastructural level, TEM showed lactate was more effective in removing minerals from the collagenous matrix, which was confirmed by SAXS analysis.
Conclusions: These findings indicated the different acids yielded lesions with different characteristics that could influence lesion formation resulting in their distinct predominance in different caries activities, and these differences may impact strategies for dentin caries remineralization.

1. Introduction

Demineralization of calcified tissues or biominerals occurs in organisms via either physiologic or pathologic processes. Physiologic demineralization such as bone resorption is an essential event in bone modeling and remodeling, tooth eruption and fracture healing, while diseases such as osteoporosis or dental caries are caused by excessive and pathologic demineralization followed by matrix degradation. Problems of human health have driven demineralization studies of calcified tissues with attention focused on the cause and characteristics of dental caries during the 19th and 20th centuries (Ehrlich, Koutsoukos, Demadis, & Pokrovsky, 2008). Knowledge of enamel caries and demineralization of enamel is substantial; in contrast, complex dentin caries and dentin demineralization need more meticulous investigations with the combination of current front-line microscopic and spectrometric techniques.

Dentin is made up of more organic components and water by volume (approximately 50%) than enamel (less than 3%). Thus, dentin caries is much more complex than enamel caries and involves at least two stages: the dissolution of biominerals by

* Corresponding author at: Department of Preventive and Restorative Dental Sciences, University of California San Francisco, San Francisco, CA 94143-0758, United States.
E-mail address: gw.marshall@ucsf.edu (G.W. Marshall).
[1] Current address: The Forsyth Institute, Department of Mineralized Tissue Biology, 245 First Street, Cambridge, MA 02142, United States.

http://dx.doi.org/10.1016/j.archoralbio.2015.10.001
0003-9969/

organic acids and the subsequent degradation of dentin matrix by proteases. In addition, natural dentin caries are geometrically complex with variations in width, depth, severity and color, making it difficult to find many similar lesions for *in vitro* studies. Artificial lesions offer significant advantages over natural lesions, since standard and reproducible lesions can be made routinely. Many attempts have been made to create artificial caries model systems using organic acids (Featherstone & Rodgers, 1981; Featherstone, Duncan, & Cutress, 1979; Featherstone, Cutress, Rodgers, & Dennison, 1982; ten Cate & Duijsters, 1982) and pH-cycling (Featherstone, 1994; Featherstone & Nelson, 1989; Featherstone, Glena, Shariati, & Shields, 1990; Featherstone, Stookey, Kaminski, & Faller, 2011; Stookey et al., 2011) to produce artificial lesions similar to natural caries. Such lesions of defined depth have also been used to evaluate various dentin remineralization procedures (Bertassoni, Habelitz, Pugach, Soares, & Marshall, 2010; Bertassoni, Habelitz, Marshall, & Marshall, 2011; Burwell et al., 2012). The changes in reduced elastic modulus (E_R) of hydrated artificial caries specimens were prepared and evaluated using an acetate buffer (pH 5) that produces a sloped mineral profile similar to natural lesions (Marshall et al., 2001; Pugach et al., 2009; Zheng, Hilton, Habelitz, Marshall, & Marshall, 2003). Noticeably deeper artificial lesions had a larger and highly demineralized outer flat zone of very low mechanical properties (Burwell et al., 2012) similar to the most severe active lesions (Burwell et al., 2012; Zheng et al., 2003). Both artificial root dentin lesions created with the same acetate buffer and natural root caries in extracted teeth have similar cross-sectional microhardness, and lesion profiles using qualitative polarized microscopy (McIntyre, Featherstone, & Fu, 2000).

While many acids or calcium chelating agents can solubilize the Ca–P crystals to create characteristic lesion models easily, acetic acid was commonly used in previous studies (Featherstone & Rodgers, 1981; Featherstone et al., 1979; Featherstone et al., 1982; Featherstone & Nelson, 1989; Featherstone et al., 1990; Featherstone et al., 2011; Stookey et al., 2011; ten Cate & Duijsters, 1982) to make artificial dentin or enamel lesions resembling natural caries. The acetate artificial caries system resulted in demineralization across the lesion similar to that observed in natural lesions of similar depths (Arends & ten Bosch, 1992). Organic acids produced by cariogenic lactobacilli are considered to play a major part in dentin demineralization (Byun et al., 2004). Distinct acids have been associated with caries activity. In active caries lactate appears to dominate, while acetate and propionate have been found in arrested carious lesions (Hojo, Komatsu, Okuda, Takahashi, & Yamada, 1994). We evaluated lesions produced by lactate and acetate buffers since the distinct association of acids with caries activities and prior work on enamel caries has shown that their demineralization characteristics may be different at the same pH (Featherstone & Rodgers, 1981).

The purpose of this study was to determine the kinetics of demineralization for two artificial dentin caries models based on lactate and acetate buffers at pH 5, a typical pH for caries demineralization, and to compare the mineral profiles and nanomechanical property profiles of large lesions of the same nominal depths produced to determine if the profiles are similar and to evaluate lesion characteristics as a foundation for their use in remineralization studies. We investigated both lesion types at the same depth (different demineralization periods) using all the analytical methods presented here for clinical relevance, as well as both lesion types demineralized at the same period of time for ultrastructural and SAXS analyses to confirm the distinct effects caused by two different acids. We sought to determine the properties of the hydrated tissue since dehydration of demineralized dentin results in shrinkage of the remaining matrix and its mechanical properties in this state do not reflect the state of the tissue *in vivo* (Bertassoni, Habelitz, Kinney, & Marshall, 2009). In addition, we investigated the ultrastructure of mineral/matrix of dentin lesions produced by these two acids, to correlate the modifications of structure to the changes of mechanical properties. The null hypothesis was that each buffer would produce similar demineralization profiles at the same pH and similar mechanical

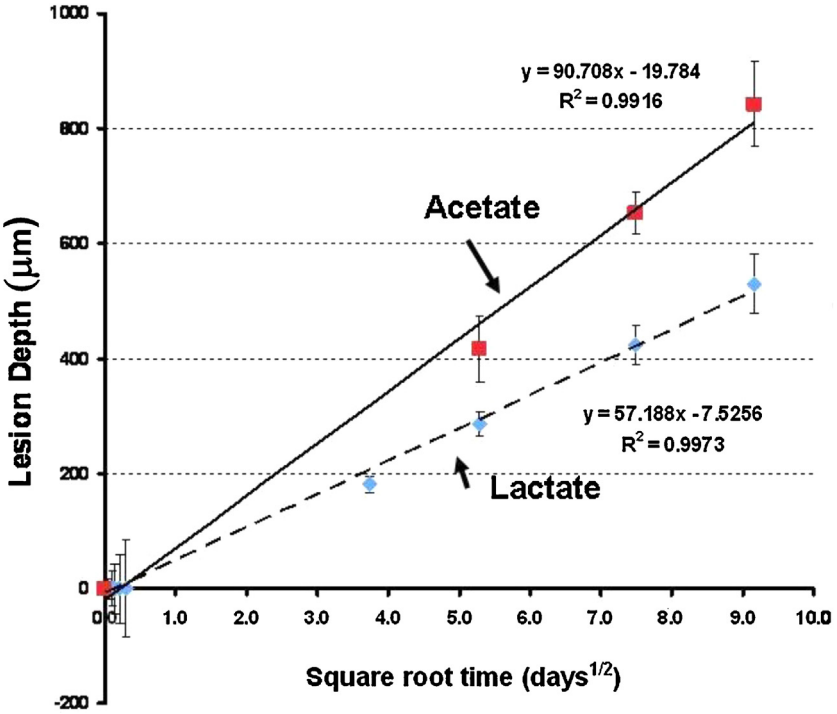

Fig. 1. Kinetic curves of dentin lesion formation (lesion depth versus square root of demineralization time) produced by acetate and lactate buffer at pH 5. Lesion depth was determined by polarized light microscope.

properties responses in lesions of the same nominal depth. Each zone of the artificial carious dentin lesions, like the corresponding zone in natural carious dentin lesions, was expected to contain residual minerals, and mechanical properties at comparable levels, and exhibit similar ultrastructural characteristics.

2. Materials and methods

2.1. Kinetics of demineralization in acetate and lactate buffers

2.1.1. Creation of artificial lesions and sample preparation

Non-carious third molars ($n > 100$) were obtained from patients requiring extraction as part of their normal dental treatments following the approved protocol. After extraction the teeth were sterilized using gamma irradiation (White, Goodis, Marshall, & Marshall, 1994) and stored in Hank's balanced salt solution at 4 °C until preparation. The enamel was removed just above the dentino-enamel junction (DEJ) using a slow-speed saw with a water cooled diamond blade (Isomet, Buehler Ltd., Lake Bluff, IL). This was achieved by making sure that fissures extended below the cut surface, leaving the surface with exposed dentin with enamel islands and enamel surrounding the dentin. The cut surfaces were carefully polished with 600-grit silicon carbide paper until an enamel island in the center of the tooth had been removed, indicating it was just below the DEJ.

A 3 mm × 3 mm window was created with acid resistant nail varnish (Revlon #270, New York, New York) centered on the area where the central enamel island had been removed. This was done to simulate an occlusal natural carious lesion in a fissure that spreads laterally and into the dentin when it reaches the DEJ. The roots were then mounted in PMMA (poly methyl methacrylate, COE Tray Plastic, Coe Laboratories, Chicago, IL) resin to prevent infiltration of the cariogenic acid through the root tip while the occlusal surface was in constant contact with the demineralization solution. Each specimen ($n = 6$/group) was placed in a 50 ml conical tube with 40 ml 0.05 M acetate or lactate buffer that contained 2.2 mM calcium and phosphate based on the recommendations by McIntyre et al. (2000). Each buffer was adjusted to pH 5.0. Demineralization solution was changed weekly for 4, 8 or 12 weeks. After the specimens had been in the artificial caries acid buffer for 4, 8 or 12 weeks, they were immediately stored in deionized water with thymol to prevent bacterial growth prior to optical imaging.

2.2. Determination of lesion depth by polarized light microscopy (PLM)

Sections about 200 μm thick were prepared through the centers of the artificial lesions for the different time points. Lesion depths were determined by polarized light microscopy (PLM) at 10X with an Olympus BX 51 microscope (Olympus America Inc., San Diego, CA). Images were collected while the lesion sections were immersed in water. Images were analyzed using ImagePro Plus software (Media Cybernetics Inc., Silver Spring, MD). Two images were captured from each sample and 5 measurements were gathered from each image, for a total of 10 measurements per sample. The demineralization kinetics were determined by plotting the measured demineralization depths against the square root of demineralization time (Fig. 1).

2.3. Lesions for nanomechanical testing and mineral content

After determination of the kinetic profiles for the two buffers, specimens were prepared following a similar procedure as described above. Dentin blocks measuring 6 mm × 3 mm × 2.5 mm were cut from the mid-coronal region of the selected teeth perpendicular to the long axis of the tooth. The specimen surfaces (the 6 mm × 3 mm occlusal faces) to be exposed to artificial caries formation were ground with SiC abrasive papers from 320 to 1200 grit, and then polished with aqueous diamond suspensions (Buehler, Lake Bluff, IL) of 6.0, 3.0, 1.0, and 0.25 μm particle sizes. Each specimen surface was covered with nail varnish (Revlon #270, New York, New York) to prevent demineralization except for a 3 × 3 mm window that was exposed for demineralization.

The specimens were demineralized at pH 5 for time periods to produce lesions from each solution that were targeted to be 40, 140 or 180 μm in depth based on the kinetic curves determined previously. Each specimen ($n = 5$/group) was placed in a 50 ml tube with 40 ml of either the lactate (exposure times of 18 h, 7d or 12d) or acetate (exposure times of 8 h, 66 h, or 130 h) demineralization solutions. Both solutions contained 0.05 M acid, 2.2 mM Ca^{2+} and PO_4^{3-} at pH 5.0. For the deep lesions, the lactate demineralization buffer was changed after 7 days. Upon removal from buffers, samples were rinsed with deionized water and stored in a 100% humid environment to maintain hydration of the demineralized tissues until studied.

2.4. Measurement of reduced elastic modulus and hardness of carious dentin by AFM-nanoindentation

Prior to the start of nanoindentation analysis, the cross-sections were hydrated in de-ionized water for one hour. Nanoindentation ($n = 5$/group) was performed in a liquid cell filled with de-ionized water using an AFM (Nanoscope III Veeco Instruments, Santa Barbara, CA) to which a load-displacement transducer (Triboscope, Hysitron Incorporated, Minneapolis, MN) was attached. A sharp diamond Berkovich indenter was calibrated on fused silica under wet conditions. The surface tension between the indenter and the liquid, including the capillary force, was taken into account during calibration that was done to obtain the actual force applied according to the detailed procedure established in our prior work (Balooch et al., 1998). Site-specific measurements of reduced elastic modulus (E_R) and hardness (H) were made using a controlled force of 350–500 μN with a 3 s trapezoidal loading curve (load, hold, and unload for 3 s each, a standard protocol in our lab group).

Each indentation yielded a load-deformation curve, from which E_R was calculated from the slope of the unloading curve and H was determined according to the following equations (Doerner & Nix, 1986):

$$E_R = \frac{\sqrt{\pi/2}}{a} \times S$$

$$H = \frac{F_{max}}{a},$$ where S represents the stiffness or slope of the unloading curve based on the method of Oliver and Pharr (Oliver & Pharr, 1992), a is the contact area of the indentation, and F_{max} is the maximum force.

Indentations were made at intervals of 4 μm starting from the epoxy embedding material just outside the surface of the lesion and proceeding inwards through the depth of the lesion and into sound dentin, covering a total distance of 300 μm (Fig. 2). This encompassed the lesion and a large region of normal dentin below the lesion. Each indentation was made in intertubular dentin. If measurements were accidentally made in areas of peritubular dentin, it was noted and not included in the calculation of intertubular dentin mechanical properties. Similar lines of indents were placed in the normal, untreated portions of the dentin specimens that had been protected by nail varnish during demineralization. The changes in mechanical properties (E_R and H) influenced by each acid demineralization treatment were analyzed following the detailed procedure by Burwell et al. (2012).

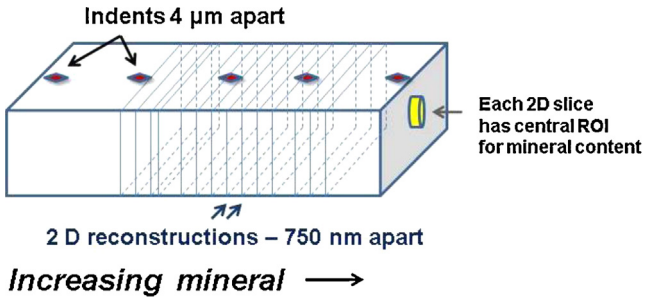

Fig. 2. Schematic of the approaches for nanoindentation and MicroXCT performed on dentin samples. Mechanical properties are obtained from nanoindentation and each nanoindent is ~500 nm deep on a surface, separated by 4 μm. Mineral profile is determined by MicroXCT, with a collection of average Hounsfield Unit (HU) in a region of interest (ROI) centered in each 750 nm 2D reconstruction.

2.5. Micro X-ray computed tomography (MicroXCT) for mineral content

Additional sagittal sections ($n = 5$/group) were imaged using MicroXCT ™, (MicroXCT-200, Xradia Inc., Pleasanton, CA) following the general procedures described by Burwell et al. (2012) and detailed in the supplemental material. Briefly, Micro XCT was carried out with a tungsten anode setting at 60 kV, 133 μA using a 10× objective and 150 μm quartz filter. The tomography data for each specimen and calibration standard (see CT scaling below) were collected at an exposure of 25 s over 1800 scans between the angles of −95° to 95° with an average spatial resolution of ~750 nm (Fig. 2) and 2000 × 2000 pixels containing 16 bit data. An averaged, multiple reference correction was collected and applied to the raw data to remove the background signal. Cross-comparison of tomographic data among specimens and conditions was achieved by transforming the linear attenuation coefficient data to the Hounsfield unit (HU) scale (Hounsfield, 2000) (See Supplemental material)

2.6. Transmission electron microscope (TEM) for ultrastructure of lesions

Selected specimens from the artificial lesion groups were evaluated by transmission electron microscopy (TEM). 70 nm thick sections were used to determine the collagen structure and selected area electron diffraction (SAED) was used to identify the nature and crystallinity of the mineral that remained in the lesions. Slices from artificial lesions from the different acids were embedded in Spurr's resin (Ted Pella, Redding, CA) after ethyl alcohol and then acetone dehydration. Selected regions were trimmed, and ultrathin sections (~70 nm) were cut in the occlusal or sagittal plane of the tissue with a diamond knife on an ultramicrotome (Reichert-Jung Ultracut E, Leica, Wetzlar, Germany). Tissue sections were placed on Formvar™ copper grids and examined in a JEOL JEM 1400 TEM (JEOL Ltd, Tokyo, Japan) at

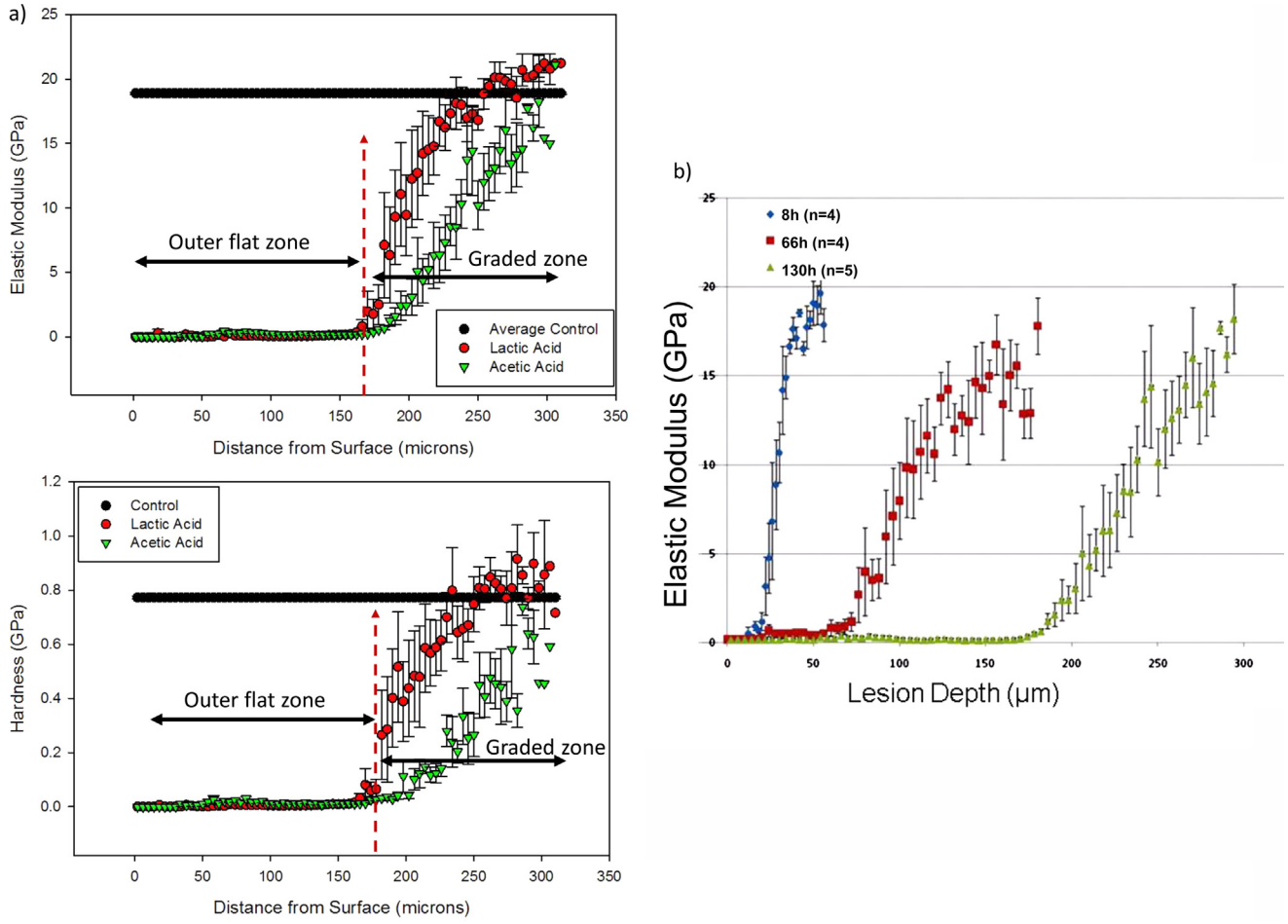

Fig. 3. (a) Elastic modulus and hardness profiles for the lesions produced by both acids with 180 μm targeted depth. (b) Average elastic modulus profiles as a function of depth for samples exposed to acetate for different times: ◇ (blue), 8 h ($n = 4$); □ (red), 66 h ($n = 4$); Δ (green), 130 h ($n = 5$). Outer zone of flat and low E_R (~0.2 GPa) increased with depth of lesions. Slope of inner graded zone decreased gradually as lesions became deeper.

an accelerating voltage of 120 kV. Images were recorded using a CCD camera (Gatan Inc., Pleasanton, CA).

2.7. Small-angle X-ray scattering (SAXS) experiments

SAXS experiments were performed at the 7.3.3 beamline of the Advanced Light Source (Lawrence Berkeley National Laboratory, Berkeley, CA, USA). Demineralized disc-shaped dentin samples ~180 μm thick were held on an aluminum sample-holder with their surface normal to the direction of the incoming X-rays. An incident radiation of 10 KeV was used with two different sample-to-detector distances of $d_{s\text{-}d1}$ = 4508 mm and $d_{s\text{-}d2}$ = 1326 mm, covering a q-range of 0.04 $nm^{-1} < q < 3$ nm^{-1}. A non-focused beam of ~1 mm × 0.5 mm size at the sample position was used. Several measurements were taken at different points of each sample to check for structural heterogeneity. Images of the scattered intensity were acquired using an ADSC Quantum 4u CCD detector with acquisition times that varied from 10 to 60 s. Tests were performed taking several scans at the same point of the sample, showing no radiation damage effects. Dark current subtraction and transmission normalization were applied to all the images before data analysis. The transmission was calculated from the values of the transmitted intensity as measured with a diode.

3. Results

3.1. Demineralization kinetics for lactate and acetate at pH 5

With the same pH and concentration, the two acids had different strengths (pK_a: acetate = 4.76, lactate = 3.86). The demineralization depths as a function of the square root of time at pH 5 are shown in Fig. 1. The linear relationship of these curves with R^2 values of more than 0.99 indicated that the demineralization was diffusion controlled. The rate of lesion progression in the acetate buffer had a much higher slope so that lesions of equivalent depth required longer demineralization in lactate than for acetate at the selected pH of 5.

3.2. Nanomechanical properties of shallow and deep artificial lesions

Fig. 2 is a schematic that compares the approaches used for nano-indentations and MicroXCT on a cross-section of dentin with a lesion. Nanoindents (500 nm deep each) were made on the top surface and E_R and H were determined along a line at intervals of 4 μm for a total length of 300 μm; whereas MicroXCT recorded the average level of x-ray attenuation in a region of interest (ROI) with intervals of 750 nm through the center of the lesion and normal dentin beneath, for a total depth of 500 μm. Fig. 3a shows the typical reduced elastic modulus and hardness profiles for the lesions with 180 μm targeted depth. Despite the similar pH and nominally similar depths, the E_R and H curves versus distance showed different nanomechanical behavior of lactate and acetate lesions. Both lesions produced an extensive outer zone of low properties (E_R~ 0.2 GPa) for a depth of about 160–170 μm followed by a sloped region of increasing stiffness towards the normal dentin. The slope was steeper for lactate than for acetate and occurred over 65 μm (E_R 0.3 GPa/μm), while acetate required a distance of 125 μm (E_R 0.16 GPa/μm) to reach normal dentin values of E_R of 20 GPa. The reduced elastic modulus profile (E_R) of three different depths of lesions, with acetate as an example, is shown in Fig. 3b. Despite the different depths, all lesions formed an outer zone of low E_R and a deeper graded zone with increasing E_R (slope of modulus) through the depth until reaching the normal dentin value. As the depth of the lesion increased, the slope of the graded zone gradually decreased (Fig. 3b). The slopes of modulus profiles for lesions of different depths are summarized in Table 1.

Table 1
Slope of modulus profile for lesions of different depths.

	Slope (GPa/μm)	
Depth (μm)	Acetate	Lactate
40	0.85	0.83
140	0.17	–
180	0.16	0.24

3.3. Mineral profiles of the deep lesions

The differences in nanomechanical properties with depth suggested that mineral profiles of the lesions might also differ for the different acids. This was investigated by MicroXCT of the deep lesions. The lesions produced by both acids displayed similar increasing trends of mineral content from the deeper part of the lesions (~100 μm) to normal dentin (Fig. 4a). The lactate-produced lesions, nevertheless, exhibited an outer (flat) zone (0–80 μm deep of lesions) with more X-ray transmission, and a zone with more gradual X-ray attenuation with increasing lesion depth, in comparison with acetate lesions. A sharp increase of X-ray absorption usually occurred at the outer edge of the acetate lesion. This suggests that abundant residual mineral was left in the acetate lesions and much less mineral remained in lactate lesions, allowing more x-ray transmission. Sagittal and occlusal 2-D virtual slices from reconstructed tomography revealed the distinct dissolution effects of different acids on dentin matrix (Fig. 4b). Lactate lesions displayed a more transparent outer (flat) zone than acetate lesions in sagittal views. In occlusal views, a remarkable swelling of lesion matrix was usually observed in lactate lesions, whereas acetate lesions retained similar dimensions to the normal dentin portions. When comparing lesion/mineral profile (MicroXCT) (Fig. 4a) and mechanical property profile from nanoindentation (Fig. 3a), it appears that the mineral profile from MicroXCT corresponded closely with the lesion depths determined from the kinetic study using PLM (Fig. 1). At the target lesion depth (in this case 170–180 μm), the value of mineral density reached that of normal dentin as expected (Fig. 4a). Lesion depths, however, appear to be deeper in mechanical properties profiles, in which the low modulus and hardness region extended beyond the 170-180 μm target depth for both acids (Fig. 3a). Thus, the low mechanical properties zone of the specimens appear to have increasing amounts of mineral although the indentation values did not increase, and significant increases in modulus and hardness only occurred after the mineral profile rose closer to the normal dentin value (Fig. 3a).

3.4. Ultrastructure of minerals and matrix in lesions under TEM

Fig. 5 shows the ultrastructure of the base of a lesion produced by lactate buffer under TEM. At low magnification (inset in Fig. 5a), an apparent “demineralization front” can be observed (white dashed curve), comparable with the 2-D radiograph by MicroXCT showing lesions distinct from the undemineralized portion of dentin (Fig. 4b). At higher magnification, however, TEM revealed the residual mineral content displayed an increasing gradient over 10 μm with depth (Fig. 5b, white dashed arrow), instead of an abrupt and clear boundary. Moreover, peritubular dentin and collagen-matrix-supported intertubular dentin were demineralized in distinct manners. In the advancing zone, substantial mineral remained in peritubular regions, consequently, dentin tubules appear torn by the shearing force during ultra-thin sectioning (Fig. 5b, damaged tubule indicated by white arrows). The surrounding intertubular dentin in this zone, nevertheless, was subjected to severe demineralization, particularly the

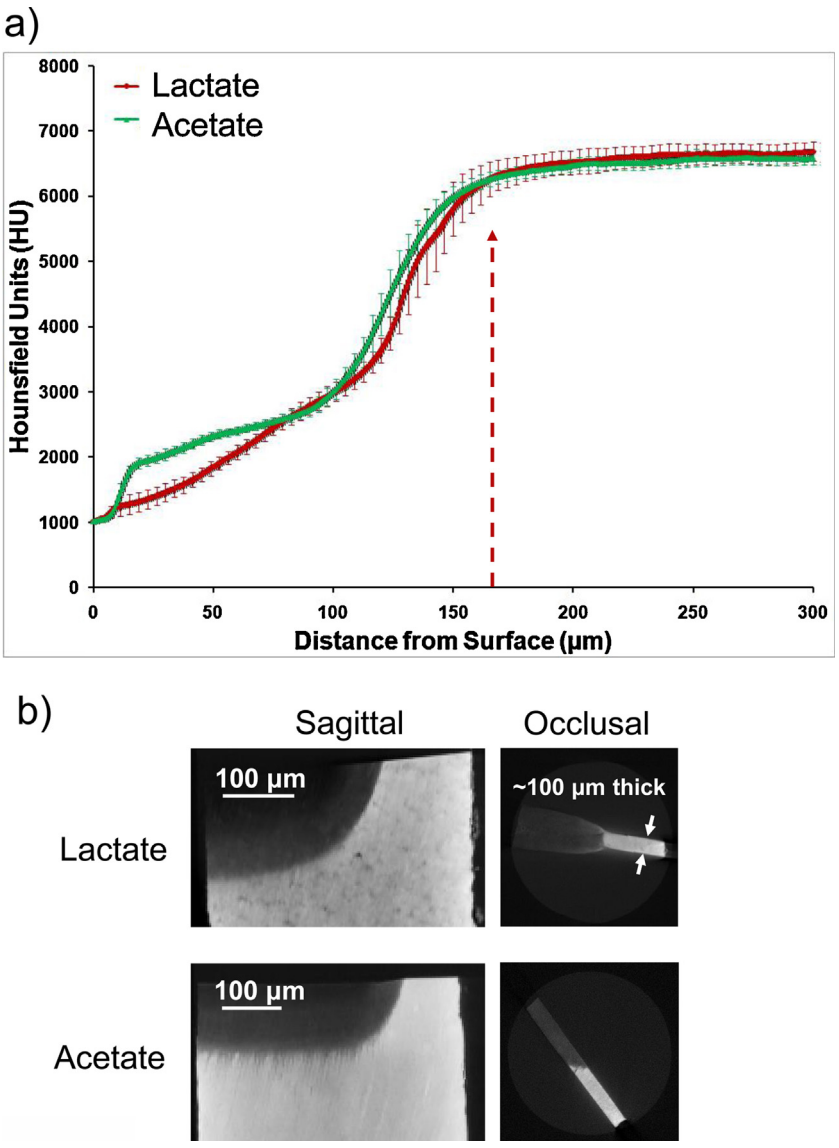

Fig. 4. Lesions with 180 μm targeted depth analyzed by MicroXCT. (a) Mineral profiles through the depth of lesions, represented by HU versus distance from surface. (b) Reconstructed sagittal and occlusal virtual slices of dentin containing lesion, showing the swelling of the matrix in lactate lesion.

intrafibrillar minerals along the collagen fibrils (Fig. 5c from the inset in Fig. 5b, collagen directions indicated by black arrows), in contrast to the densely mineral-filled normal dentin (Fig. 5d).

TEM imaging revealed remarkable differences in ultra-structure in the lesions produced by the two different acids (Figs. 6 and 7). Comparing the margin and the outer portion of both types of lesions, the acetate buffer lesions still contain significant amounts of residual minerals (Fig. 6a and c). Note that even the remnant of the peritubular dentin seems to contain some remaining mineral. Lactate removed most of the minerals in the lesion matrix (Fig. 6b), leaving discernible collagen fibrils (black arrow) with typical periodicity of type I collagen at about 60–70 nm (Fig. 6d, black arrow and inset, unstained section). At the deeper regions of lesions (Fig 7, sloped zone or close by regions), acetate dissolved peritubular mineral more efficiently than lactate did, and a circle of membranous protein always remained in each tubule lumen (compare Fig. 7a and b, block arrow indicates the membranous matrix). In acetate buffer, the matrix-guided intertubular dentin generally demineralized incompletely, leaving behind needle- and splinter-like crystallites (inset in Fig. 7c). Lactate dissolved minerals much more slowly than acetate and preferentially along collagen fibrils (Fig 7d, collagen directions indicated by black arrows).

3.5. Small Angle X-ray scattering results

Due to the different demineralization kinetics of the two acids, the demineralization time to produce equivalent depth of lesions was very different. To evaluate if demineralization time induced the observed difference in efficacy of mineral dissolution by the two acids, we prepared dentin discs ~180 μm thick and demineralized them for 3 weeks in either acetate or lactate buffer, presumably enough time to demineralize the dentin disc evenly and completely. After demineralization, we performed SAXS analysis on these samples.

SAXS results are presented in Fig. 8 as scattered intensity, a.u. (absolute units (cm^{-1})) *vs* scattering vector, q (Liss, Bartels, Schreyer, & Clemens, 2003) (or k by Fratzl and colleagues (Fratzl, Fratzl-Zelman, & Klaushofer, 1993)). The graph in Fig. 8a shows the simulated SAXS intensity of a model dilute system of disk-shaped particles with a mono-dispersed radius of 485 nm and polydispersed thickness of 2.4 nm (the polydispersity function is a

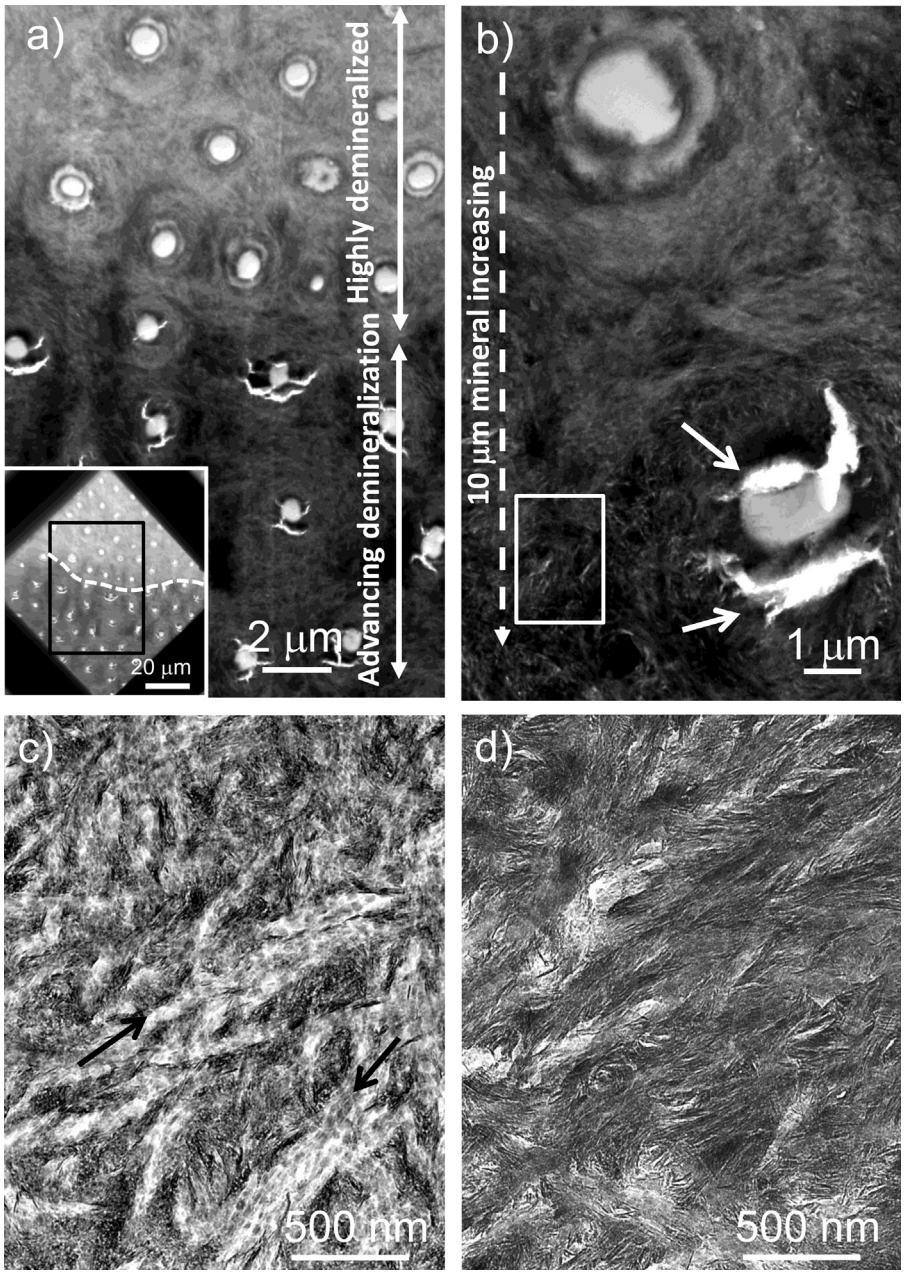

Fig. 5. Ultrastructure of the base of a lesion. Low magnification image (inset in a) shows an apparent "demineralization front", but higher magnification reveals that the demineralization proceeding from a highly demineralized part into an advancing zone. Tubules in the advancing zone were torn during ultra-thin sectioning as substantial amount of minerals still remain in peritubular and intertubular regions (a and b). Preferential dissolution occurred along collagen fibrils and showing etched intrafibrillar minerals (in c), in contrast to the fully mineralized normal dentin (in d).

Gaussian function with $\sigma = 0.96$ nm). The SAXS intensity of an isotropic dilute system of disk-shaped particles is characterized by a Porod region (i.e., high q domain (Sinha, Sirota, Garoff, & Stanley, 1988)) with a q^{-2} slope between two positions in q that are characteristic of the radius and the thickness of the particles, respectively. Figure 8b shows the SAXS curves for three demineralized dentin samples (demineralized with EDTA, acetate and lactate buffers, respectively) after 3 weeks of demineralization at pH 5. We used EDTA as a positive control, since it has been reported (Gerstenfeld, Feng, Gotoh, & Glimcher, 1994) that EDTA is more efficient than acids in releasing 95% of the total calcium content after 48 h. It also provides gentle dissolution preventing matrix degradation via inhibiting protease activation and reducing commonly encountered artifacts of tissue shrinkage obtained with rapid decalcification by acids. The acetic acid demineralized dentin shows a change of slope at $q \sim 1.8\,\text{nm}^{-1}$, which is attributed to particle scattering by disk-shaped particles (the curve in Fig. 8a qualitatively reproduces this curve). Based on previous experience from time-resolved collagen remineralization SAXS experiments (unpublished data), we can attribute this particle scattering to collagen mineralization by calcium phosphate in the form of platelet- or disk-shaped particles, typical of intrafibrillar apatite (Fratzl, Fratzl-Zelman, Klaushofer, Vogl, & Koller, 1991; Fratzl, Groschner, Vogl, Eschberger, & Fratzl-Zelman, 1992; Fratzl et al., 1993; Marten, Fratzl, Paris, & Zaslansky, 2010). The radius of the disk-shaped particles cannot be determined from this data due to the absence of a clear change in the slope at low q. The dentin sample demineralized with lactic acid had a profile with a constant slope underlying the peaks of the collagen d-band structure from different orders of the 0 0 l reflection ($l = 2$, 4.. etc.) The $l = 1$, 3..

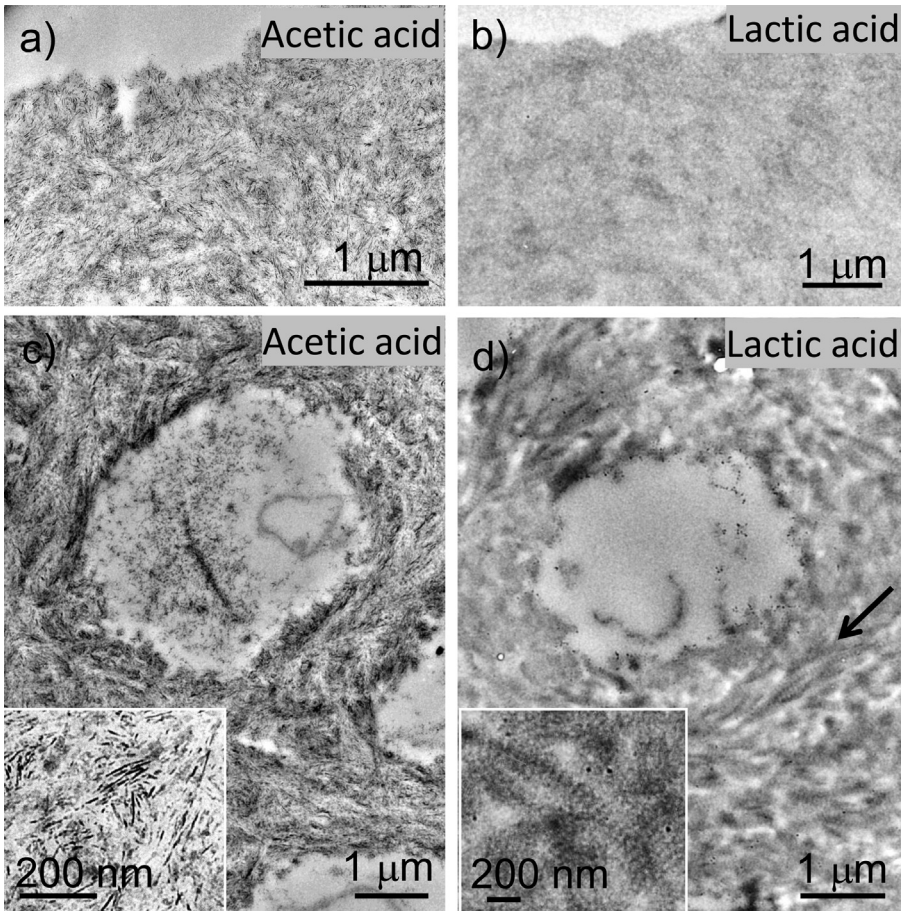

Fig. 6. Margin and the outer portion of lesions under TEM (a: acetate lesion, and b: lactate lesion). Plenty of residual minerals remained in acetate lesions (c and inset). Lactate removed most of the minerals in the outer portion of the lesion (in b and d), exposing visible collagen fibrils (arrow) with 60–70 nm periodicity of type I collagen (in d, arrow and inset, all unstained section).

reflections were hidden by the signal from residual apatite platelets. The lack of clear particle scattering in this curve and the visible collagen d-band structure peaks suggest that this sample has a lower level of mineralization than that demineralized with acetate buffer. The sample demineralized with EDTA shows no traces of particle scattering (no mineral left in the collagen) and a clear signature of the collagen d-band structure ($l = 2, 3, 4..$ etc. $l = 1$ is out of the experimental q range). Fig. 8c shows pure collagen from rat-tail tendon displaying strong peaks from different orders of the 0 0 l reflection ($l = 1, 2, 3..$ etc.) of the d-band structure of pure collagen. The periodicity of the d-band structure can be obtained from the slope of a plot of the q-position of each reflection as a function of its reflection order (see inset in Fig. 8c). No obvious changes in d-band of collagen in EDTA and lactate lesions were observed. For the rat-tail tendon, a collagen d-band structure with periodicity $p = 64.7$ nm was obtained in the dry condition.

4. Discussion

4.1. Unique demineralization process in dentin lesion

In enamel lesion studies, it has been debatable whether artificial lesions were created via diffusion-controlled (Featherstone & Rodgers, 1981), or surface-controlled mechanism (Hoppenbrouwers & Driessens, 1988; Margolis & Moreno, 1990; Margolis, Zhang, Lee, & Moreno, 1999). In this dentin lesion work, we demonstrated that the production of artificial dentin lesions at pH 5 by acetic or lactic acids, commonly found in natural caries, is controlled by a diffusion mechanism, as shown in Fig. 1. Acetic acid exhibits a linear kinetic relationship with steeper slope, i.e., faster kinetics in dentin lesion production, than lactic acid. Our evaluations further identified variations in artificial dentin lesions in their ultrastructure, profile of mechanical properties and distinct effects induced by two different acids.

Using polarized light microscopy, artificial lesions produced by both acids generally showed well-defined lesion boundaries with normal dentin beneath (data not shown), and the measurement of lesion depth is from the top of the lesion surface to the boundary. MicroXCT displayed the lesions with clear visual boundaries between demineralized and mineralized dentin that were similar to optical images, with funnel-shaped tubules discernible under higher magnification (e.g. Fig. 4b). The funnel shape resulted from opening the tubule lumen as peritubular dentin was demineralized as the tubules act as channels for acids to pass through the “base” of lesion into mineralized dentin. (Fig. 4b). In this deeper part, however, the attenuation coefficient was similar to the level of normal dentin, despite the visible broader tubules (Fig. 4a). TEM imaging is capable of a wide range of magnification to observe macro- to ultra-structure, and showed that not only was the peritubular dentin demineralized, but permeation of acids occurred beyond the lesion “base” in adjacent intertubular compartment. The lesion “base” viewed under an optical microscope (Fig. 1) or 2-D radiograph (Fig. 4b) is similar to the “demineralization front” of the low magnification TEM image (inset in Fig. 5a). At higher magnification progressive dissolution was apparent beyond the “demineralization front” and, dissolution

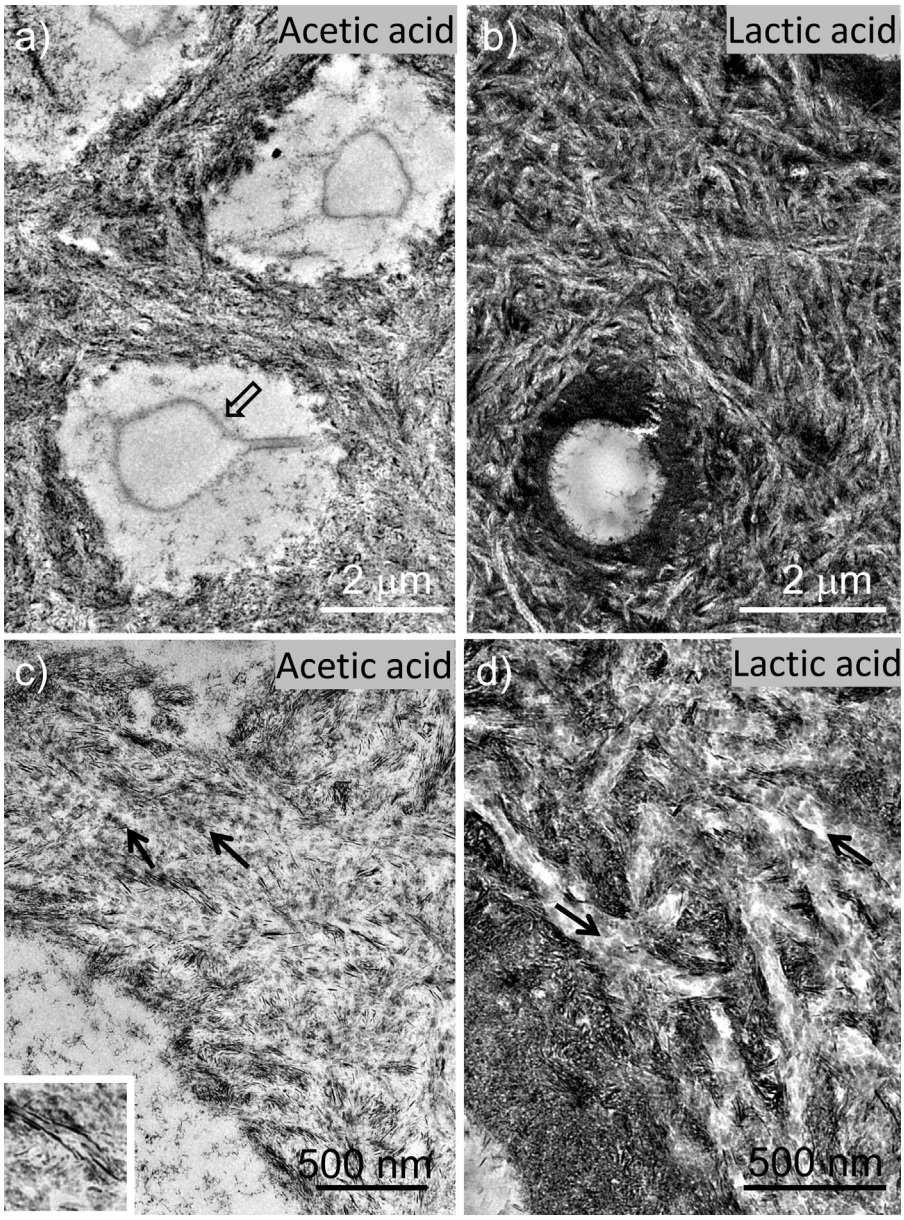

Fig. 7. Ultra-structure of the deeper regions of lesions (sloped zone) produced by either acetate (a and c) or lactate buffers (b and d). Peritubular dentin was dissolved more in the acetate lesion than in the lactate lesion (compare a and b). Lactic acid dissolves slower than acetate and preferentially along collagen fibrils (compare c and d).

progressed in both peritubular and intertubular dentin. Noticeably, demineralization advanced further intrafibrillarly along collagen fibrils to form a roughly negative silhouette of dentin matrix network (Fig. 7b and d), even though abundant mineral within peritubular dentin remained. The progression of dentin lesions appeared to be guided by the dentin matrix network.

The profile of mechanical properties in these artificial dentin lesions is consistent with TEM ultrastructural observation that the depth of lesions extends further, beyond the apparent lesion "base" in optical or MicroXCT images. Elastic modulus or hardness profiles of an artificial dentin lesion characteristically consist of a flat zone (~0.2 GPa) and a graded zone (from 0.2 GPa to the value of normal dentin) through the depth (Fig. 3a). The outer flat zone matches the target lesion depth from the kinetic curves (e.g. dashed red lines in Figs. 3 and 4a). It is of interest to compare the characteristics of these artificial lesions with natural lesions. In prior work (Zheng et al., 2003) natural lesions were classified as moderately active and inactive. Nanoindentation results (see Fig. 3) showed a clear difference in the two classes with the more active having a very low modulus or soft outer zone and a relatively steeper rise to normal dentin values. This resembles the curves in the current study and we hypothesize that a recycling model might lead to a gentler slope as in the less active lesions. In addition, the microstructures seen in the different zones resembled the structures seen in the natural lesions as shown in the 2003 study and in more detail in the study by Pugach et al. (Pugach et al., 2009). Specifically, the flat outer portion of artificial lesions has much or all of the peritubular dentin removed, and the sloped zone tends to have remnants of peritubular dentin, and the deeper zone that has near normal modulus appears to be normal dentin. The artificial lesions do not however have typical transparent dentin layer found in the natural lesions. Comparison of the lesions mineral (Fig. 4a) and mechanical property (Fig 3a) profiles, shows much more mineral to the left of the dashed red line than would be expected from the modulus profile. One reason for this may be that a critical mineral level must be reached before the indentation force can be resisted (Bertassoni

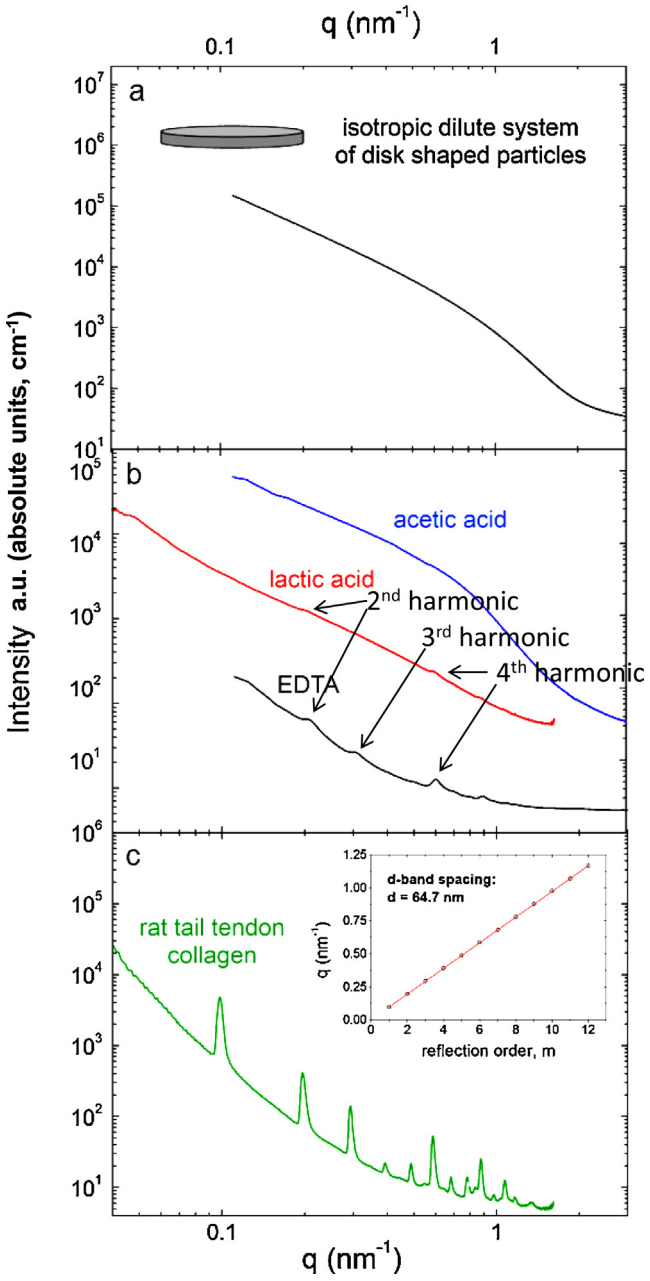

Fig. 8. SAXS analysis of demineralized dentin disc shows that the acetic acid lesion contains residual minerals and the scattering curve approximately follows that of disc-shaped particles, while lactic acid is more efficient in removing minerals, with reference to the curve of complete demineralized dentin disc by EDTA. (a) A scattering curve of disc-shaped particle system, (b) dentin lesions produced by acetate, lactate, and EDTA demineralization, (c) scattering curve of rat tail tendon collagen with diffraction from collagen d-banding of 64 nm at dry condition. (For interpretation of the references to color in the text, the reader is referred to the web version of this article.)

et al., 2009). Under TEM, a highly demineralized part of the lesion corresponded to the flat zone in the modulus profile, while the advancing zone with a demineralization gradient provided an increasing modulus profile (Fig. 5a). This graded zone may arise out of matrix-guided permeation of the acid to produce the intrafibrillar demineralization. Dentin is a composite-like material with its mineral and matrix constructing a "graded ultrastructure" at the nanoscale where gradual changes of interphases within minerals or matrix components, or sudden changes at the matrix and mineral interfaces, could variably modify the physicochemical and functional properties of the composite material (Weiner, Nudelman, Sone, Zaslansky, & Addadi, 2006). It is sensible that the dissolution kinetics and reactivity of biominerals in dentin lesions will differ in the extrafibrillar and intrafibrillar compartments of dentin matrix due to different matrix-mineral interfaces and gradient changes in composition and structure. Moreover, intrafibrillar biominerals may be more soluble, owing to their thermodynamic properties modulated by incorporation and substitution of foreign ions (thus increasing lattice strains and distorting the crystal lattice (De Yoreo & Vekilov, 2003; Koutsoukos, 1998; Kibby & Hall, 1972; Pokroy et al., 2006), and their crystal size confined and distorted by the protein fibrils (Orgel et al., 2001; Orgel, Irving, Miller, & Wess, 2006; Perumal, Antipova, & Orgel, 2008). In fact, although the size and shape of minerals in bone or dentin remain debatable due to the limitation of measuring techniques and sample preparation (Kinney et al., 2001a; Kinney, Pople, Marshall, & Marshall, 2001b), intrafibrillar minerals are generally reported to be more uniform and of smaller size than extrafibrillar minerals in dentin or bone (in length, intrafibrillar: 40–50 nm; extrafibrillar: 30-200 nm (Alexander et al., 2012; Eppell, Tong, Katz, Kuhn, & Glimcher, 2001; Kinney et al., 2001b; Tong, Glimcher, Katz, Kuhn, & Eppell, 2003).

Organic-mineral surface interactions are commonly considered to inhibit dissolution exclusively at mineral surfaces (Weiner & Dove, 2003). Natural biominerals, nevertheless, have also been known to undertake unusual etching/dissolution promoted and/or guided by mineral-occluded macromolecules or matrix networks. For example, it has been shown in the calcite system that unusual and accelerated dissolutions of biogenic calcite were caused by matrix network occluded in organic hydrogel-grown calcite crystals (Estroff, Addadi, Weiner, & Hamilton, 2004), and in avian eggshell when the shell was resorbed for the needs of the embryonic development (Chien, Hincke, & McKee, 2009). More relevant to this study, enamel of deciduous teeth has been shown to contain higher organic content than permanent teeth (Mortimer, 1970; Müller & Schmitz-Feuerhake, 1998). Consequently, they are more susceptible to acid etching that could contribute to higher caries rates than permanent teeth (Angker, Nockolds, Swain, & Kilpatrick, 2004; Hunter, West, Hughes, Newcombe, & Addy, 2000; Wang, Tang, Bonstein, Bush, & Nancollas, 2006). Similar phenomena have been observed in demineralization of bone. Weakly dissociated organic acids and their buffers generally produced a rapidly penetrating diffuse attack on bone mineral (Birkedal-Hansen, 1974; Eggert & Germain, 1979). These examples support the concept that organic matrix networks can provide pathways for acid molecules to diffuse. In the present study of dentin lesions, we suggest that the acid buffers etch intrafibrillar minerals faster than the surrounding extrafibrillar minerals (Figs.5 c and 7) due to protein guidance.

4.2. Acetate and lactate buffers produced different dentin lesions

At the macroscopic level, acetic and lactic acids vary in their kinetics of producing dentin lesions (Fig. 1). The dissociation constant for lactic acid is about one unit smaller than acetic acid (lactic acid: 3.86, acetic acid: 4.76). At pH 5 and equal molarity, lactic acid presents in aqueous solution in a more dissociated form than acetic acid, which means more acidic in general. The faster kinetics of lesion production by the less acidic acid may be enlightened to some extent, if not completely, by our multiple high-resolution microscopic methods analyzing composite-like dentin at the nanoscale.

Modulus (E_R) and hardness profiles of two different types of lesions show that acetate buffer created graded zones of lower slope than lactate (for lactate the graded zone occurred over 65 μm (0.3 GPa/μm), while for acetate it occurred over a distance of

125 μm (0.16 GPa/μm)). This fits the model proposed by Featherstone and Rodgers (1981) that weak acids diffuse faster in tissue (in their case enamel) in un-ionized form acetate creates artificial dentin lesions and diffuses faster and deeper beyond the lesion "base", as visualized by TEM showing more extensive extra- and intra-fibrillar demineralization, as well as in the peritubular dentin despite numerous residual crystallites (Fig. 7a and c).

Residual crystallites left in acetate lesions (even at the most demineralized areas) could arise from a kinetic size-effect at nanoscale level during the dissolution of biominerals. Nancollas and co-workers discovered that the dissolution of biominerals can be self-hindered and even fully suppressed owing to nanometric size of crystallites (Wang et al., 2005). In their studies of enamel lesion formation, the surfaces of enamel persist undissolved in water (pH 5.5–5.8) despite undersaturation (Tang, Wang, & Nancollas, 2004a; Tang et al., 2004b). As active etch pits on the dissolving surfaces formed and spread, only the pits larger than a critical size will contribute to dissolution. A crystallite smaller than the critical size will no longer dissolve and can be stabilized, thus exerting a level of crystallite persistence. These residual crystallites smaller than the critical size were not susceptible to dissolution (unless a significant drop of pH occurred) and may be stabilized in the fluctuating acetate buffer.

Conversely, given the kinetic size effect of the nanocrystallites, it is rather remarkable that a weak acid like lactic acid is capable of removing most of the minerals, similar to EDTA and distinct from acetic acid. In their study of enamel caries formed by acetate and lactate, Hoppenbrouwers and Driessens (1988) proposed that specific adsorption of the acid anions to the mineral can moderate the dissolution of minerals and affect the progression of the lesion depth. Yoshioka et al. further suggested that acidic anions interaction with bone apatite involve more than one stage (Yoshioka et al., 2002). At first, acid anions adsorb on mineral surfaces to form calcium-anion complex. In the second stage, the acid anions will either stay attached to the biomineral surfaces with only limited dissolution, or the calcium–anion complex will detach and initiate substantial decalcification, depending upon the diffusion rate of the calcium–anion complexes into solution. Lactate is a known chelating agent (Cariati, Morazzoni, Zanderighi, Marcotrigiano, & Pellacani, 1977; Lu et al., 1992) comparable to citric acid, and is often used in chelation therapy clinically. It is likely that lactic anions chelate on the residual nanocrystallites in dentin matrix, resulting in further demineralization. Future study of how the dissolution kinetics of dentin biominerals influenced by the specific adsorption of acetic and lactic anions onto the minerals may give additional insight into this scenario. Besides the anion-adsorption scenario, the size of acid molecules may be an ancillary factor influencing the diffusion behavior, given the same concentration of acids. Since a molecule's diffusion rate is roughly inversely proportional to its size (Brogioli & Vailati, 2001), undissociated acetic acid molecules should have 0.4–0.5 times faster diffusion rate, than lactic acid molecules.

Our MicroXCT and TEM results clearly showed that lactate seemed to loosen or open the dentin matrix that resulted in swelling of the hydrated tissue (Fig. 4, MicroXCT, 2-D virtual slices, which corresponded well to the continuous slope of attenuation coefficient profile for lactate lesions, in contrast to a sudden increase in attenuation at the water-lesion interface for acetate lesions) and dissolved most of the minerals without residual crystallites (TEM, Fig. 6, outer part of lesions). SAXS analysis further confirmed these results, on the baseline of the same demineralization time for lesions produced by either acid: residual minerals in acetate-treated samples (blue curve in Fig. 8b) yield a particle scattering curve typical of a platelet/disc shape (a typical curve of disc-shaped particle scattering is shown in Fig. 8a), whereas lactic acid is more efficient in removing minerals and exposing collagen fibrils, and revealing some of the scattering peaks of the collagen periodicity (red curve in Fig. 8b) with reference to the curves of samples complete demineralized by EDTA (black curve in Fig. 8b) and pure rat tail collagen (green curve in Fig. 8c). After SAXS analysis, the same samples were prepared for ultra-structural investigation under TEM. The results (data not shown) displayed very similar ultrastructure to the margin and outer portion of artificial lesions on dentin blocks, i.e., the flat zone (Fig. 6). This suggests that the lesion formation kinetics determined by the lesion depth is not predictive of ability to remove all the minerals. This also implies that lactate buffer is capable of removing the minerals in dentin lesions completely, perhaps owing to its more acidic nature (lower dissociation constant), slower kinetics and some possible secondary demineralization mechanism (Yoshioka et al., 2002). While collagen matrix and non-collagenous proteins are unlikely to be degraded by both acids (Ehrlich et al., 2008), this more complete demineralization by lactic acid may be followed by destruction of the collagenous matrix by activation of host-derived endogenous proteases, e.g. multiple metalloproteinases (MMPs), including MMP-8, MMP-2, and MMP-9 (Chaussain-Miller, Fioretti, Goldberg, & Menashi, 2006; Martin-De Las Heras, Valenzuela, & Overall, 2000; Tjaderhane et al., 1998; van Strijp, Jansen, DeGroot, ten Cate, & Everts, 2003), that could lead to the swollen matrix visualized under MicroXCT. Particularly, in the dental caries process, cariogenic lactic acid may permeate along the collagen matrix network, likely activating MMPs at acidic pH, followed by collagen destruction at neutralized pH due to the local demineralization along collagen (Chaussain-Miller et al., 2006; Tjaderhane et al., 1998).

5. Conclusions

In conclusion, dentin lesions were created by organic weak acids demineralization via diffusion of un-ionized acid molecules, which appeared to be guided by collagen fibrils. This matrix-guided demineralization process may also operate in other collagenous calcified tissues such as bone. Acetic acid diffused faster into lesions than lactic acid, due to the larger amount of un-ionized acetic acid, which is about 10 times that of lactic acid at pH 5.0. In addition, lactic acid was more effective than acetic acid in removing biominerals in dentin (even at the same, prolonged demineralization time), resulting in the more disorganized matrix structure and the steeper increase of mechanical properties in lactate lesions near the lesion depth. This result agrees with the observed ultrastructure of natural active caries lesions where lactate is the major acid (Sarnat & Massler, 1965).

Ethics statement

The study is approved by UCSF CHR (UCSF Committee on Human Research). Teeth were collected in accord with IRB policy that did not require written consent for the collection of tooth specimens that did not have personal identifying data.

Acknowledgements

Research reported in this publication was supported by the National Institute of Dental and Craniofacial Research of the National Institutes of Health under grant number R01DE016849. Additional support was provided by NIH/NCRR S10RR026645 for MicroXCT and CTSI-SOS Grant Award # 000166 for AFM and nanoindentation. Fellowship support was provided for Y-C Chien by Fonds de recherche en santé du Québec (FRSQ). SAXS studies were carried out at the Advanced Light Source at Lawrence Berkeley National Laboratory and were supported by the Director, Office of Science, Office of Basic Energy Sciences, of the U.S.

Department of Energy under Contract No. DE-AC02-05CH11231. Conceived and designed the experiments: YCC, AB, KS, JDF, SJM, GWM. Performed the experiments: YCC, AB, KS, AFM, MKP, GN, MRH. Analyzed the data: YCC, AB, KS, AFM, MKP, SH, SPH. Wrote the paper: YCC, AB, AFM, MKP. Edited and contributed interpretation: KS, SH, SPH, JDF, SJM, GWM.

Appendix A. Supplementary data

Supplementary data associated with this article can be found, in the online version, at http://dx.doi.org/10.1016/j.archoralbio.2015.10.001.

References

Ehrlich, H., Koutsoukos, P. G., Demadis, K. D., & Pokrovsky, O. S. (2008). Principles of demineralization: Modern strategies for the isolation of organic frameworks Part I. Common definitions and history. *Micron*, *39*(December (8)), 1062–1091 PubMed PMID: WOS:000260873600002.

Featherstone, J. D., Duncan, J. F., & Cutress, T. W. (1979). A mechanism for dental caries based on chemical processes and diffusion phenomena during in-vitro caries simulation on human tooth enamel. *Archives of Oral Biology*, *24*(2), 101–112 PubMed PMID: 299136.

Featherstone, J. D., & Rodgers, B. E. (1981). Effect of acetic, lactic and other organic acids on the formation of artificial carious lesions. *Caries Research*, *15*(5), 377–385 PubMed PMID: 6942921.

Featherstone, J. D., Cutress, T. W., Rodgers, B. E., & Dennison, P. J. (1982). Remineralization of artificial caries-like lesions in vivo by a self-administered mouthrinse or paste. *Caries Research*, *16*(3), 235–242 PubMed PMID: 6954001.

ten Cate, J. M., & Duijsters, P. P. (1982). Alternating demineralization and remineralization of artificial enamel lesions. *Caries Research*, *16*(3), 201–210 PubMedPMID: 6953998.

Featherstone, J. D., & Nelson, D. G. (1989). Recent uses of electron microscopy in the study of physico-chemical processes affecting the reactivity of synthetic and biological apatites. *Scanning Microscopy*, *3*(September (3)), 815–827 PubMed PMID: 2617263, discussion 27–8.

Featherstone, J. D., Glena, R., Shariati, M., & Shields, C. P. (1990). Dependence of in vitro demineralization of apatite and remineralization of dental enamel on fluoride concentration. *Journal of Dental Research*, *69*(2) Spec No: 620–5; discussion 34–6, PubMed PMID: 2312892.

Featherstone, J. D. (1994). Fluoride, remineralization and root caries. *American Journal of Dentistry*, *7*(October (5)), 271–274 PubMed PMID: 7986451.

Featherstone, J. D., Stookey, G. K., Kaminski, M. A., & Faller, R. V. (2011). Recommendation for a non-animal alternative to rat caries testing. *American Journal of Dentistry*, *24*(October (5)), 289–294 PubMed PMID: 22165456.

Stookey, G. K., Featherstone, J. D., Rapozo-Hilo, M., Schemehorn, B. R., Williams, R. A., Baker, R. A., et al. (2011). The Featherstone laboratory pH cycling model: a prospective, multi-site validation exercise. *American Journal of Dentistry*, *24*(October (5)), 322–328 PubMed PMID: 22165462.

Bertassoni, L. E., Habelitz, S., Pugach, M., Soares, P. C., Marshall, S. J., & Marshall, G. W. Jr. (2010). Evaluation of surface structural and mechanical changes following remineralization of dentin. *Scanning*, *32*(September–October (5)), 312–319 PubMed PMID. 20853406. Pubmed Central.

Bertassoni, L. E., Habelitz, S., Marshall, S. J., & Marshall, G. W. (2011). Mechanical recovery of dentin following remineralization in vitro—an indentation study. *Journal of Biomechanics*, *44*(January (1)), 176–181 PubMed PMID. 20926080. Pubmed Central.

Burwell, A. K., Thula-Mata, T., Gower, L. B., Habelitz, S., Kurylo, M., Ho, S. P., et al. (2012). Functional remineralization of dentin lesions using polymer-induced liquid-precursor process. *PLoS One*, *7*(6), e38852 PubMed PMID: 22719965. Pubmed Central.

Marshall, G. W., Habelitz, S., Gallagher, R., Balooch, M., Balooch, G., & Marshall, S. J. (2001). Nanomechanical properties of hydrated carious human dentin. *Journal of Dental Research*, *80*(August (8)), 1768–1771 PubMed PMID: WOS.000174683800017 (English).

Zheng, L., Hilton, J. F., Habelitz, S., Marshall, S. J., & Marshall, G. W. (2003). Dentin caries activity status related to hardness and elasticity. *European Journal of Oral Sciences*, *111*(June (3)), 243–252 PubMed PMID: 12786956.

Pugach, M. K., Strother, J., Darling, C. L., Fried, D., Gansky, S. A., Marshall, S. J., et al. (2009). Dentin caries zones: mineral, structure, and properties. *Journal of Dental Research*, *88*(January (1)), 71–76 PubMed PMID: 19131321. Pubmed Central..

McIntyre, J. M., Featherstone, J. D. B., & Fu, J. (2000). Studies of dental root surface caries. 1: comparison of natural and artificial root caries lesions. *Australian Dental Journal*, *45*(March (1)), 24–30 PubMed PMID: WOS.000086342100006. English.

Arends, J., & ten Bosch, J. J. (1992). Demineralization and remineralization evaluation techniques. *Journal of Dental Research*71 Spec No: 924–8. PubMed PMID: 1592988.

Byun, R., Nadkarni, M. A., Chhour, K. L., Martin, F. E., Jacques, N. A., & Hunter, N. (2004). Quantitative analysis of diverse Lactobacillus species present in advanced dental caries. *Journal of Clinical Microbiology*, *42*(July (7)), 3128–3136 PubMed PMID. 15243071. Pubmed Central.

Hojo, S., Komatsu, M., Okuda, R., Takahashi, N., & Yamada, T. (1994). Acid profiles and pH of carious dentin in active and arrested lesions. *Journal of Dental Research*, *73*(December (12)), 1853–1857 PubMed PMID: 7814758.

Bertassoni, L. E., Habelitz, S., Kinney, J. H., Marshall, S. J., & Marshall, G. W. Jr. (2009). Biomechanical perspective on the remineralization of dentin. *Caries Research*, *43*(1), 70–77 PubMed PMID: 19208991. Pubmed Central.

White, J. M., Goodis, H. E., Marshall, S. J., & Marshall, G. W. (1994). Sterilization of teeth by gamma radiation. *Journal of Dental Research*, *73*(September (9)), 1560–1567 PubMed PMID: 7929992.

Balooch, M., Wu-Magidi, I. C., Balazs, A., Lundkvist, A. S., Marshall, S. J., Marshall, G. W., et al. (1998). Viscoelastic properties of demineralized human dentin measured in water with atomic force microscope (AFM)-based indentation. *Journal of Biomedical Materials Research*, *40*(June (4)), 539–544 PubMed PMID: 9599029.

Doerner, M. F., & Nix, W. D. (1986). A method for interpreting the data from depth-sensing indentation instruments. *Journal of Materials Research*, *1*(04), 601–609.

Oliver, W. C., & Pharr, G. M. (1992). An improved technique for determining hardness and elastic-modulus using load and displacement sensing indentation experiments. *Journal of Materials Research*, *7*(June (6)), 1564–1583 PubMed PMID: WOS:A1992HY10600033.

Hounsfield, G. N. (2000). Computed Medical Imaging Science. 1980;210(4465):22-8. PubMed PMID: WOS:A1980KJ 3708. *English*.J3708.

Liss, K.-D., Bartels, A., Schreyer, A., & Clemens, H. (2003). High-energy X-rays: a tool for advanced bulk investigations in materials science and physics. *Textures and Microstructures*, *35*(3–4), 219–252 2003/09/01.

Fratzl, P., Fratzl-Zelman, N., & Klaushofer, K. (1993). Collagen packing and mineralization. An X-ray scattering investigation of turkey leg tendon. *Biophysical Journal*, *64*(January (1)), 260–266 PubMed PMID. 8431546. Pubmed Central.

Sinha, S. K., Sirota, E. B., Garoff, S., & Stanley, H. B. (1988). X-ray and neutron-scattering from rough surfaces. *Physical Review B*, *38*(August (1)), 2297–2311 PubMed PMID: WOS:A1988P706700010.

Gerstenfeld, L. C., Feng, M., Gotoh, Y., & Glimcher, M. J. (1994). Selective extractability of noncollagenous proteins from chicken bone. *Calcified Tissue International*, *55*(September (3)), 230–235 PubMed PMID: 7987738.

Fratzl, P., Fratzl-Zelman, N., Klaushofer, K., Vogl, G., & Koller, K. (1991). Nucleation and growth of mineral crystals in bone studied by small-angle X-ray scattering. *Calcified Tissue International*, *48*(June (6)), 407–413 PubMed PMID: 2070275.

Fratzl, P., Groschner, M., Vogl, G., Plenk, H. Jr., Eschberger, J., Fratzl-Zelman, N., et al. (1992). Mineral crystals in calcified tissues: a comparative study by SAXS. *Journal of Bone and Mineral Research*, *7*(March (3)), 329–334 PubMed PMID: 1585835.

Marten, A., Fratzl, P., Paris, O., & Zaslansky, P. (2010). On the mineral in collagen of human crown dentine. *Biomaterials*, *31*(July (20)), 5479–5490 PubMed PMID: 20399496.

Hoppenbrouwers, P. M., & Driessens, F. C. (1988). The effect of lactic and acetic acid on the formation of artificial caries lesions. *Journal of Dental Research*, *67*(December (12)), 1466–1467 PubMed PMID: 3198843.

Margolis, H. C., & Moreno, E. C. (1990). Physicochemical perspectives on the cariostatic mechanisms of systemic and topical fluorides. *Journal of Dental Research*, *69*(February), 34–36 PubMed PMID: 2179321, Spec No: 606–13; discussion.

Margolis, H. C., Zhang, Y. P., Lee, C. Y., Kent, R. L. Jr., & Moreno, E. C. (1999). Kinetics of enamel demineralization in vitro. *Journal of Dental Research*, *78*(July (7)), 1326–1335 PubMed PMID: 10403460.

Weiner, S., Nudelman, F., Sone, E., Zaslansky, P., & Addadi, L. (2006). Mineralized biological materials: A perspective on interfaces and interphases designed over millions of years. *Biointerphases*, *1*(June (2)), P12–P14 PubMed PMID: ISI:000203008100002.

Pokroy, B., Fitch, A. N., Marin, F., Kapon, M., Adir, N., & Zolotoyabko, E. (2006). Anisotropic lattice distortions in biogenic calcite induced by intra-crystalline organic molecules. *Journal of Structural Biology*, *155*(July (1)), 96–103 PubMed PMID: 16682231.eng..

Kibby, C. L., & Hall, W. K. (1972). Surface properties of calcium phosphates. In M. L. Hair (Ed.), *The Chemistry of Biosurface II* (pp. 663–729).New York: Marcel Dekker.

Koutsoukos, P. G. (1998). Influence of metal ions on the crystal growth of calcium phosphates. In Z. Amjad (Ed.), *Calcium Phosphates in Biological and Industrial Systems* (pp. 145–171).Kluwer Academic Publishers.

De Yoreo, J. J., & Vekilov, P. G. (2003). Principles of crystal nucleation and growth, 1st ed. In P. M. Dove, J. J. De Yoreo, & S. Weiner (Eds.), *Biomineralization. Reviews in Mineralogy and Geochemistry:* (Vol. 54. pp. 57–93).Washinton, D.C: The Mineralogical Society of America.

Orgel, J. P., Miller, A., Irving, T. C., Fischetti, R. F., Hammersley, A. P., & Wess, T. J. (2001). The in situ supermolecular structure of type I collagen. *Structure*, *9*(November (11)), 1061–1069 PubMed PMID: 11709170.

Orgel, J. P., Irving, T. C., Miller, A., & Wess, T. J. (2006). Microfibrillar structure of type I collagen in situ. *Proceedings of the National Academy of Sciences of the United States of America*, *24*(June (24)), 9001–9005 PubMed PMID: 16751282. Pubmed Central..

Perumal, S., Antipova, O., & Orgel, J. P. (2008). Collagen fibril architecture, domain organization, and triple-helical conformation govern its proteolysis. *Proceedings of the National Academy of Sciences of the United States of America*, *105*(February (26)), 2824–2829 PubMed PMID: 18287018. Pubmed Central..

Kinney, J. H., Pople, J. A., Driessen, C. H., Breunig, T. M., Marshall, G. W., & Marshall, S. J. (2001a). Intrafibrillar mineral may be absent in dentinogenesis imperfecta type II (DI-II). *Journal of Dental Research*, *80*(June (6)), 1555–1559 PubMed PMID: 11499512.

Kinney, J. H., Pople, J. A., Marshall, G. W., & Marshall, S. J. (2001b). Collagen orientation and crystallite size in human dentin: a small angle X-ray scattering study. *Calcified Tissue International*, *69*(July (1)), 31–37 PubMed PMID: 11685431.

Eppell, S. J., Tong, W., Katz, J. L., Kuhn, L., & Glimcher, M. J. (2001). Shape and size of isolated bone mineralites measured using atomic force microscopy. *Journal of Orthopaedic Research*, *19*(November (6)), 1027–1034 PubMed PMID: 11781001.

Tong, W., Glimcher, M. J., Katz, J. L., Kuhn, L., & Eppell, S. J. (2003). Size and shape of mineralites in young bovine bone measured by atomic force microscopy. *Calcified Tissue International*, *72*(5), 592–598 PubMed PMID: 12724830.

Alexander, B., Daulton, T. L., Genin, G. M., Lipner, J., Pasteris, J. D., Wopenka, B., et al. (2012). The nanometre-scale physiology of bone: steric modelling and scanning transmission electron microscopy of collagen-mineral structure. *Journal of the Royal Society Interface*, *9*(August (73)), 1774–1786 PubMed PMID: 22345156. Pubmed Central..

Weiner, S., & Dove, P. M. (2003). An overview of biomineralization processes and the problem of the vital effect, 1st ed. In P. M. Dove, J. J. De Yoreo, & S. Weiner (Eds.), *Biomineralization. Reviews in Mineralogy and Geochemistry:* (Vol. 54. pp. 1–29). Washinton, D.C: The Mineralogical Society of America.

Estroff, L. A., Addadi, L., Weiner, S., & Hamilton, A. D. (2004). An organic hydrogel as a matrix for the growth of calcite crystals. *Organic & Biomolecular Chemistry*, *2* (January (1)), 137–141 PubMed PMID: 14737673. Epub 2004/01/23. eng..

Chien, Y. C., Hincke, M. T., & McKee, M. D. (2009). Ultrastructure of avian eggshell during resorption following egg fertilization. *Journal of Structural Biology*, *168* (December (3)), 527–538 PubMed PMID: 19595771.

Mortimer, K. V. (1970). The relationship of deciduous enamel structure to dental disease. *Caries Research*, *4*(3), 206–223 PubMed PMID: 5270190. Epub 1970/01/01.eng.

Comparison between deciduous and permanent teeth in relation to their utility for EPR dosimetry. R. Müller, & I. Schmitz-Feuerhake (Eds.). *Proceedings of the International Workshop on the German Society for Radiation Protection 19969–12*.

Angker, L., Nockolds, C., Swain, M. V., & Kilpatrick, N. (2004). Quantitative analysis of the mineral content of sound and carious primary dentine using BSE imaging. *Archives of Oral Biology*, *49*(2), 99–107 PubMed PMID: 14693203. Epub 2003/12/25.eng.

Hunter, M. L., West, N. X., Hughes, J. A., Newcombe, R. G., & Addy, M. (2000). Erosion of deciduous and permanent dental hard tissue in the oral environment. *Journal of Dentistry*, *28*(May (4)), 257–263 PubMed PMID: 10722899. Epub 2000/03/21.eng.

Wang, L. J., Tang, R., Bonstein, T., Bush, P., & Nancollas, G. H. (2006). Enamel demineralization in primary and permanent teeth. *Journal of Dental Research*, *85* (April (4)), 359–363 PubMed PMID: 16567559. Epub 2006/03/29.eng..

Birkedal-Hansen, H. (1974). Kinetics of acid demineralization in histologic technique. *Journal of Histochemistry & Cytochemistry*, *22*(June (6)), 434–441.

Eggert, F. M., & Germain, J. P. (1979). Rapid demineralization in acidic buffers. *Histochemistry*, *59*(3), 215–224 1979/09/01 (English).

Wang, L., Tang, R., Bonstein, T., Orme, C. A., Bush, P. J., & Nancollas, G. H. (2005). A new model for nanoscale enamel dissolution. *The Journal of Physical Chemistry B*, *109*(2), 999–1005 2005/01/01.

Tang, R., Wang, L., & Nancollas, G. H. (2004a). Size-effects in the dissolution of hydroxyapatite: an understanding of biological demineralization. *Journal of Materials Chemistry*, *14*(14), 2341–2346.

Tang, R., Wang, L., Orme, C. A., Bonstein, T., Bush, P. J., & Nancollas, G. H. (2004b). Dissolution at the nanoscale: self-preservation of biominerals. *Angewandte Chemie International Edition*, *43*(20), 2697–2701.

Yoshioka, M., Yoshida, Y., Inoue, S., Lambrechts, P., Vanherle, G., Nomura, Y., et al. (2002). Adhesion/decalcification mechanisms of acid interactions with human hard tissues. *Journal of Biomedical Materials Research*, *59*(1), 56–62.

Cariati, F., Morazzoni, F., Zanderighi, G. M., Marcotrigiano, G., & Pellacani, G. C. (1977). Chelating properties of lactate anion. perturbing effect of additional ligands on bis(-lactato)-metal(II) complexes. *Inorganica Chimica Acta*, *21*(0), 133–140.

Lu, L., Singh, J. S., Galperin, M. Y., Drake, D., Taylor, K. G., & Doyle, R. J. (1992). Chelating agents inhibit activity and prevent expression of streptococcal glucan-binding lectins. *Infection and Immunity*, *60*(9), 3807–3813 PubMed PMID: 1500189. Pubmed Central.

Brogioli, D., & Vailati, A. (2001). Diffusive mass transfer by nonequilibrium fluctuations: Fick's law revisited. *Physical Review E Statistical Nonlinear and Soft Matter Physics*, *63*(January (1 Pt 1)), 012105 PubMed PMID: 11304296.

Tjaderhane, L., Larjava, H., Sorsa, T., Uitto, V. J., Larmas, M., & Salo, T. (1998). The activation and function of host matrix metalloproteinases in dentin matrix breakdown in caries lesions. *Journal of Dental Research*, *77*(8), 1622–1629 PubMed PMID: 9719036.

Martin-De Las Heras, S., Valenzuela, A., & Overall, C. M. (2000). The matrix metalloproteinase gelatinase A in human dentine. *Archives of Oral Biology*, *45*(9), 757–765.

van Strijp, A. J. P., Jansen, D. C., DeGroot, J., ten Cate, J. M., & Everts, V. (2003). Host-derived proteinases and degradation of dentine collagen in situ. *Caries Research*, *37*(1), 58–65.

Chaussain-Miller, C., Fioretti, F., Goldberg, M., & Menashi, S. (2006). The role of matrix metalloproteinases (MM Ps) in human caries. *Journal of Dental Research*, *85*(1), 22–32 PubMed PMID: 16373676.

Sarnat, H., & Massler, M. (1965). Microstructure of active and arrested dentinal caries. *Journal of Dental Research*, *44*(November (6)), 1389–1401.